

# Effect of Heat Input on M-A Constituent and Toughness of Coarse Grain Heat-Affected Zone in an X100 Pipeline Steel

Xiao-Nan Wang, Yan-Jun Zhao, Peng-Fei Guo, Xiao-Nan Qi, Hong-Shuang Di, Min Zhang, and Chang-Jun Chen

(Submitted January 19, 2018; in revised form October 24, 2018; published online February 14, 2019)

The joining of 14.8 mm thick pipeline steels was achieved with developments in high-power fiber laser by laser welding or hybrid laser arc welding. However, there were few studies on the effects of single-pass welding heat input on the M-A component and impact toughness of the heat-affected zone. In this study, single-pass welding thermal cycle was performed on Gleeble 3800 thermal simulation tester; the effect of heat input on microstructure, M-A constituent, hardness, toughness and corrosion resistance of coarse-grained heat-affected zone of X100 pipeline steel was studied. The results showed: The microstructure was lath martensite with a heat input of less than 8 kJ/cm. When the heat input was 26–36 kJ/cm, the microstructure was granular bainite. The heat input had not obvious effect on hardness (only 16% hardness reduction in this heat input arrange). However, the impact toughness was strongly influenced by heat input, with an 88% hardness reduction compared to base metal, due to M-A constituent and prior austenite grain size. Few finer M-A constituent dispersing in austenite was obtained instead of necklace-like M-A constituent at the prior austenite grain boundary when the welding heat input was less than 15 kJ/cm, which was beneficial to improve the impact toughness and corrosion resistance of welded joints of X100 pipeline steels.

**Keywords** impact toughness, M-A constituent, microstructure, pipeline steel, welding thermal cycle

## 1. Introduction

With the consumption of energy source such as petroleum and natural gas increasing, the extraction has been extended from inland to offshore, deep sea and frigid Arctic (Ref 1). Under long-distance and high-pressure conditions, pipeline transmission was one of the most important ways to deal with the above issues, and it developed toward high strength and large diameter in order to save the operation costs and improved transmission efficiency (Ref 2). Relevant studies showed that natural gas transmission capacity was increased from 100 to 300 million to 30 billion cube/year and reduced the operation costs by 30% using ultra-high strength X100 instead

of X70 pipeline steels. Thus, X100 pipeline steel was possible to be the primary materials for the transmission of petroleum and natural gas in the future (Ref 3).

X100 pipeline had a 174 J of impact energy at 20 °C temperatures, and its yield and tensile strength were 690–840 MPa and 760–990 MPa, respectively (Ref 4). Welding was the essential process to the production and assembly of pipelines such as multi-pass submerged arc welding, gas shielded welding. The fine microstructure of base metal was coarsened during welding thermal cycle, which leads to the deterioration of mechanical properties of welded joints. (Ref 5–7). Thus, many researchers have made many valuable results on the evolution of microstructure and properties during double-pass welding thermal cycle process through thermal simulation test using multi-pass submerged arc welding (Ref 8–12). The results showed that the inter-critically coarse-grained heat-affected zone (IC-CGHAZ) was the primary issue in the welding of pipeline steels, which toughness cannot meet requirements because of the presence of necklace M-A constituents forming near the prior austenite grain boundaries (PAGB).

Using single-pass welding, IC-CGHAZ of X100 pipeline steel was absent, and it was possible to solve the problem that the toughness of X100 welded joints cannot meet the requirements. With the rapid development of high-power laser, laser welding or hybrid fiber laser arc welding provided a new method to realize the single-pass welding of X100 pipeline steel with a thickness of 14.8 mm (Ref 13, 14). However, the CGHAZ was the vulnerable region for the properties of welded joints in single-pass welding. Thus, this present paper studied the evolution of microstructure and properties of CGHAZ of X100 pipeline steel with different heat inputs using thermal simulation test, including grain size, hardness, impact fracture morphology and secondary crack. The study on the relationship

**Xiao-Nan Wang**, Ministry-Province Jointly-Constructed Cultivation Base for State Key Laboratory of Processing for Non-Ferrous Metal and Featured Materials, Nanning 530004 Guangxi, People's Republic of China; and Shagang School of Iron and Steel, Soochow University, Suzhou 215021, People's Republic of China; **Yan-Jun Zhao**, Ministry-Province Jointly-Constructed Cultivation Base for State Key Laboratory of Processing for Non-Ferrous Metal and Featured Materials, Nanning 530004 Guangxi, People's Republic of China; **Peng-Fei Guo**, **Min Zhang**, and **Chang-Jun Chen**, Shagang School of Iron and Steel, Soochow University, Suzhou 215021, People's Republic of China; and **Xiao-Nan Qi** and **Hong-Shuang Di**, State Key Laboratory of Rolling and Automation of Northeastern University, Shenyang 110819, People's Republic of China. Contact e-mail: wxn@suda.edu.cn.

between microstructure and properties will provide a theoretical basis for the formulation of welding parameters in laser welding or hybrid laser arc welding of X100 pipeline steels.

## 2. Experimental Procedures

### 2.1 Materials

Table 1 lists the chemical composition of X100 pipeline steel. It was smelted ingot in 150 kg vacuum smelting furnace and then forged. Hot rolling was implemented on  $\phi$  450 mm using hot rolling experimental mill. The heating temperature of experimental steel was 1250 °C. The rolling process consisted of rough rolling and finish rolling; the steel plate was rolled from 120 to 50 mm experienced three passes during rough rolling. The start temperature and finish temperature were 1200 and 1050 °C, respectively. With the temperature cooled to 870 °C, the finish rolling was performed and the thickness was reduced from 50 to 12 mm experiencing five passes. During finish rolling process, the finish temperature was 820-840 °C, and then, the surfaces of steel plates were injection water cooled to 400-440 °C with a cooling rate of 25 °C/s. Figure 1 presents the microstructure of experimental steel. It consisted of bainite and a few fine M-A constituent dispersing on the bainitic ferrite matrix (B). The yield and tensile strength of experimental steel was 730 MPa and 835 MPa, respectively. The elongation was ~ 20%.

### 2.2 Methods

The welding thermal simulation test of samples with a size of 80 × 11 × 11 mm was carried out using Gleeble 3800 thermal simulation test machine. The samples were heated to 1350 °C with a heating rate of 100 °C/s and hold for 1 s; the different welding heat inputs were obtained by adjusting the values of  $t_{8/5}$  (3, 5, 10, 15, 30 and 60 s). The relationship between heat input and  $t_{8/5}$  is given in formula (1) (Ref 15):

$$E = d \sqrt{\frac{4\pi\lambda c\rho t_{8/5}}{\left[\left(\frac{1}{500-T_0}\right)^2 - \left(\frac{1}{800-T_0}\right)^2\right]}} \quad (\text{Eq 1})$$

where  $E$  is welding heat input (J/cm),  $d$  is actual thickness of welded plates (cm), here is 1.48,  $\lambda$  is thermal conductivity (W/(cm·°C)), the value is 0.42,  $c$  is specific heat capacity (J/(cm·°C)), the value is 0.5,  $\rho$  is density of experimental steel (g/cm<sup>3</sup>), the value is 7.8,  $T_0$  is initial temperature or initial ambient temperature (°C), its value is 25 °C. According to Eq 1, the calculated heat input was 8, 10, 15, 18, 26 and 36 kJ/cm, respectively. Figure 2 presents the thermal cycle curves under different heat input conditions according to the formula (1).

After thermal simulation, the samples were prepared by mechanical processing into 55 × 10 × 10 mm with a “V”-notch in the center. The impact toughness at - 40 °C

**Table 1 Chemical composition of X100 pipeline steel (mass fraction, %)**

C	Si	Mn	Al	Ti	Cr	Mo	Nb	Fe
0.06	0.25	1.93	0.025	0.02	0.20	0.25	0.05	Bal.

temperature was tested using ZBC-300 pendulum impact testing machine, and the average value was obtained by three repeated experiments. SU5000 scanning electron microscope (SEM) was used to observe the impact fracture surface. Samples were polished and etched with 4% nital and then, the microstructure and crack on the side of fracture were observed by Zeiss Axio Vert.A1 optic microscope (OM) and SEM. M-A constituent was etched with Lepera reagents (4% picral and 1%Na<sub>2</sub>S<sub>2</sub>O<sub>5</sub>) and observed by OM. The prior austenite grain boundary was etched with 15% picric aqueous solution and then to be observed by OM. The area fraction of M-A constituent and prior austenite grain size were counted by software of Image Pro-Plus 6.0 (IPP software) with ten images in each condition.

The corrosion resistance of experimental steel was estimated using VersaSTAT 4 electrochemical workstation with different heat inputs at room temperature. Three-electrode method was selected in this study: Platinum electrode was as auxiliary electrode, a saturated calomel electrode was as reference electrode and the simulated steels under different heat inputs were as working electrode. The size of sample was 10 × 10 mm. Mixed solution of NaHCO<sub>3</sub> (0.5 mol/L) and NaCl (0.02 mol/L) was used in electrochemical test, with an electrode area of 1 cm<sup>2</sup>. Pre-polarization was performed to

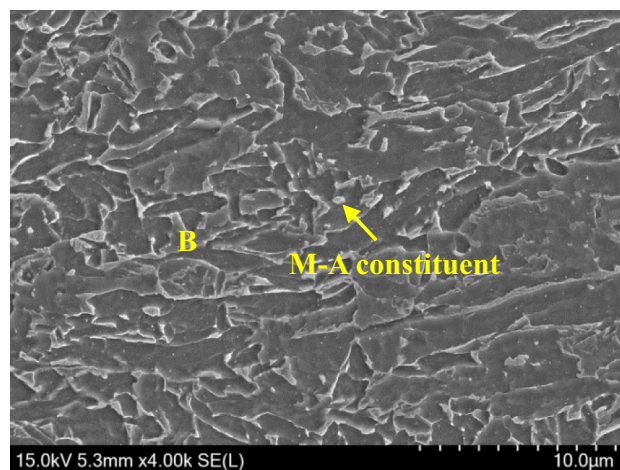


**Fig. 1** Microstructure of experimental steel

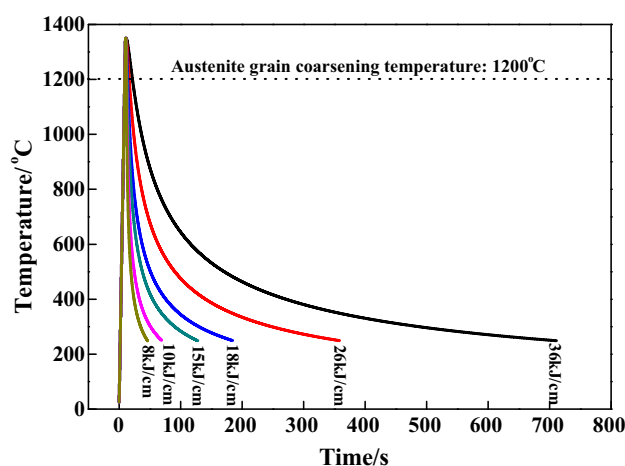


**Fig. 2** Welding thermal cycle curve with different heat inputs

remove the oxidation film on the sample surface before testing potentiodynamic polarization curve. The working electrode was stationary in solution for 0.5 h and then, potentiodynamic polarization was carried out at the scanning speed of 0.5 mV/s; scanning potential range was  $-0.95$ - $1.0$  V.

### 3. Results and Discussion

#### 3.1 Effect of Heat Input on Microstructure and Prior Austenite Grain Size of CGHAZ

Figure 3 presents the microstructure of CGHAZ with different heat inputs. When the heat input was 8-18 kJ/cm,

the microstructure consisted of lath bainite (LB) and granular bainite (GB) (Fig. 3a-d), and the content of LB was decreasing with the heat input increased (Ref 13). When the heat input was 26-36 kJ/cm, the microstructure was only GB (Fig. 3e-f). Based on the phase transformation mechanism, it can be inferred that the microstructure was LB when the heat input was less than 8 kJ/cm, but it was GB in the case of a heat input of 36 kJ/cm and more.

Figure 4 presents the prior austenite grain morphology with different heat inputs, and their effect relation is presented in Fig. 5. Fine prior austenite grain was observed when the heat input was 8 kJ/cm, but it was coarsened significantly with the increasing heat input. Statistical analysis was done using linear intercept method and ten photographs were selected for each

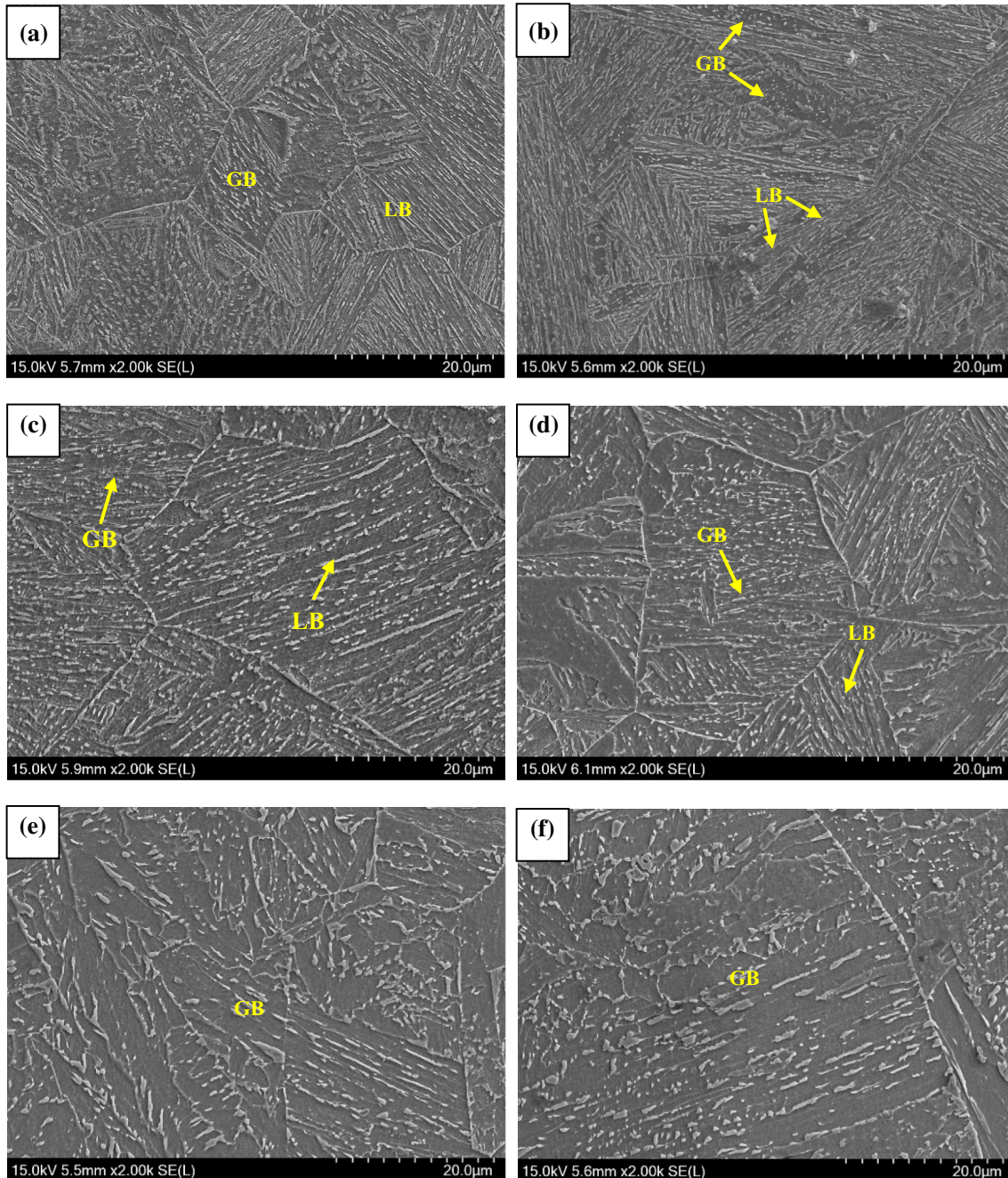


**Fig. 3** Microstructure of CGHAZ with different heat inputs. (a) 8 kJ/cm; (b) 10 kJ/cm; (c) 15 kJ/cm; (d) 18 kJ/cm; (e) 26 kJ/cm; (f) 36 kJ/cm

heat input. The results showed that the austenite grain size was only  $\sim 17 \mu\text{m}$  when the heat input was 8 kJ/cm, and it was  $\sim 100 \mu\text{m}$  as the heat input increased to 36 kJ/cm. In previous studies, it was confirmed that austenite coarsening temperature was 1200 °C for X100 pipeline steel with Nb (Ref 16). Thus, the prior austenite size was strongly influenced by the hold time at high temperature during welding thermal cycle process in this study. From Fig. 2, when the heat input was 8, 10, 15, 18, 26 and 36 kJ/cm, the hold time of more than 1200 °C was 2.68, 3.03, 3.89, 4.75, 7.35 and 12.61 s, respectively. With the heat input increased, the austenite grain boundary had enough time to occur migrate. As a result, the grain size was coarsened.

Exponential relationship was taken and fitted by origin software as listed in formula (2):

$$D = 0.76 * e^{(E/7.65)} + 15.7 \quad (\text{Eq 2})$$

where  $D$  is prior austenite grain size ( $\mu\text{m}$ ),  $E$  is welding heat input (kJ/cm). For the samples with large size ( $55 \times 10 \times 10 \text{ mm}$ ), it was difficult to simulate laser/laser arc hybrid welding with low heat input ( $< 8 \text{ kJ/cm}$ ) using current thermal simulation test machine, since the welding speed cannot achieve  $10^3 \text{ }^\circ\text{C/s}$ . Thus, it was difficult to obtain the simulated microstructure with a lower heat input due to limit cooling rate on this thermal simulation machine, but the

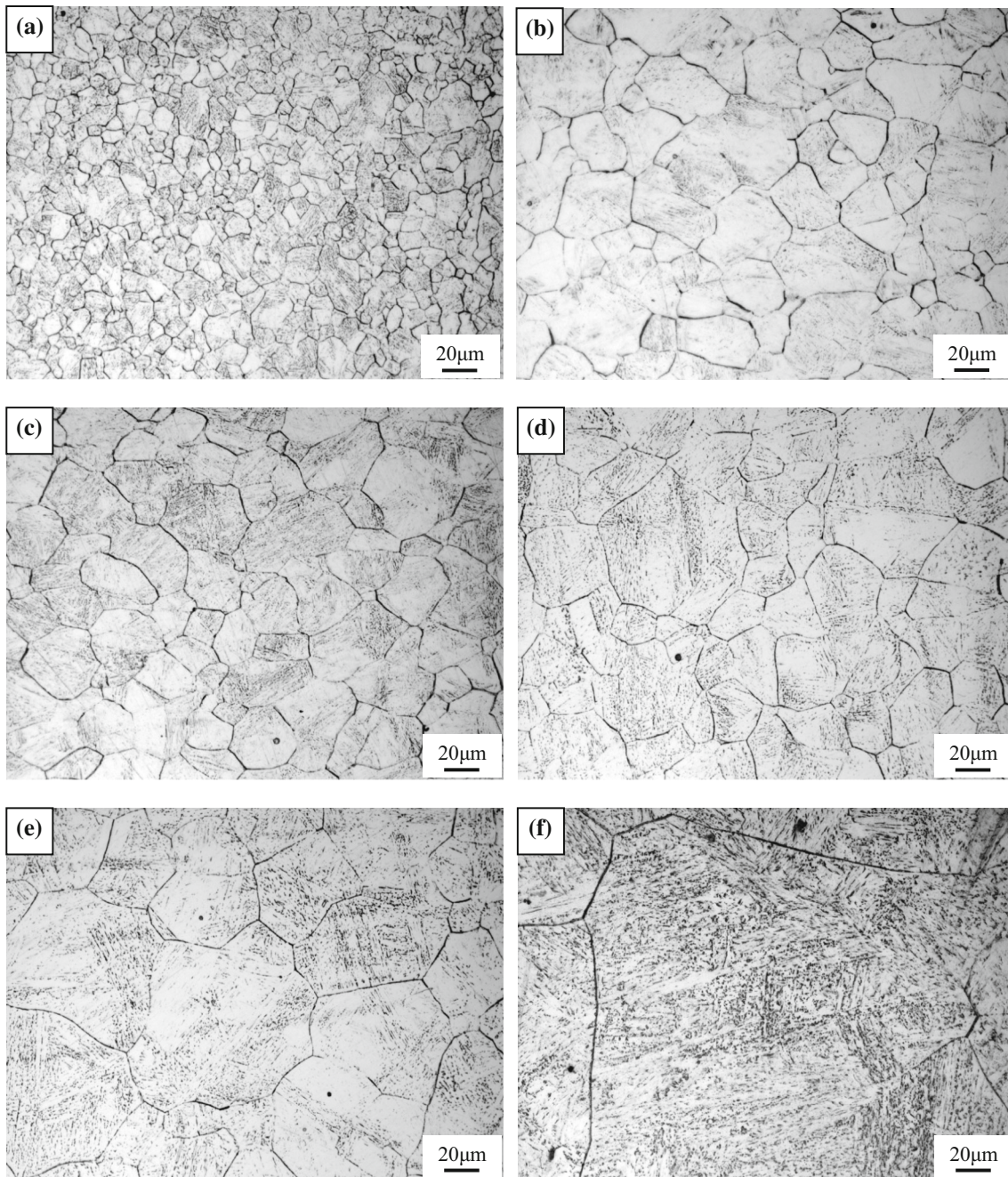


**Fig. 4** Prior austenite grain of CGHAZ with different heat inputs. (a) 8 kJ/cm; (b) 10 kJ/cm; (c) 15 kJ/cm; (d) 18 kJ/cm; (e) 26 kJ/cm; (f) 36 kJ/cm

prior austenite grain size of CGHAZ can be estimated by formula (2).

In order to verify the accuracy of this established mathematical model and welding-simulated microstructure, X100 pipeline steel with a 7 mm thick was welded using IPG YLR-6000 fiber laser. The laser power was 6000 W with a focus of – 10 mm. Different heat inputs (1.0, 1.2 and 1.5 kJ/cm) were obtained when the welding speed was 60, 50 and 40 mm/s. The microstructure of CGHAZ during laser welding was similar to the simulated results, consisted of lath bainite (Fig. 6). The measured prior austenite grain size was 17.2, 17.8 and 19.9  $\mu\text{m}$ , respectively. In the same heat inputs, the calculated values in Eq 2 were 16.5, 16.5 and 16.6  $\mu\text{m}$ , respectively. Thus, Eq 2 was effective to predict the prior austenite grain size of CGHAZ based on thermal simulation test. Moreover, the thermal simulation microstructure can provide an important basis for predicting the microstructure of laser/laser arc hybrid welding.

### 3.2 Effect of Heat Input on Size and Fraction of M-A Constituent

Figure 7 presents the distribution of M-A constituent (light microstructure, etched by Lepera reagent) in CGHAZ with different heat inputs.

When the heat input was 8 and 10 kJ/cm, M-A constituent dispersed in the prior austenite grain and between the bainite ferrite laths (Fig. 7a and b), only a few was on the prior austenite grain boundaries (PAGB). With the heat input increased to 15-36 kJ/cm, the M-A constituent on PAGB was increased (as indicated by yellow arrows in Fig. 7c-f), and its spacing was gradually decreased to form a necklace shape.

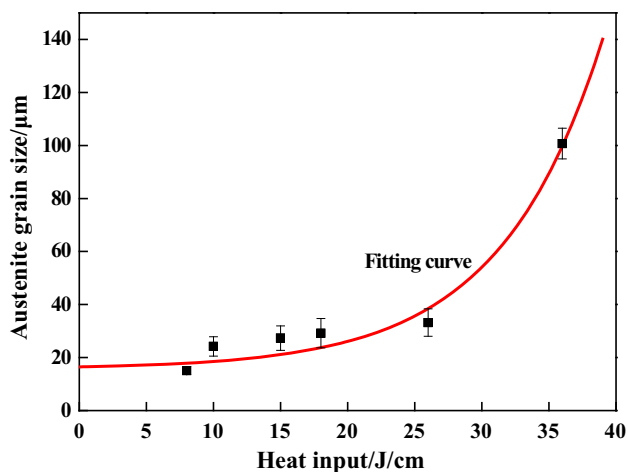


Fig. 5 Effect of heat input on the prior austenite grain size

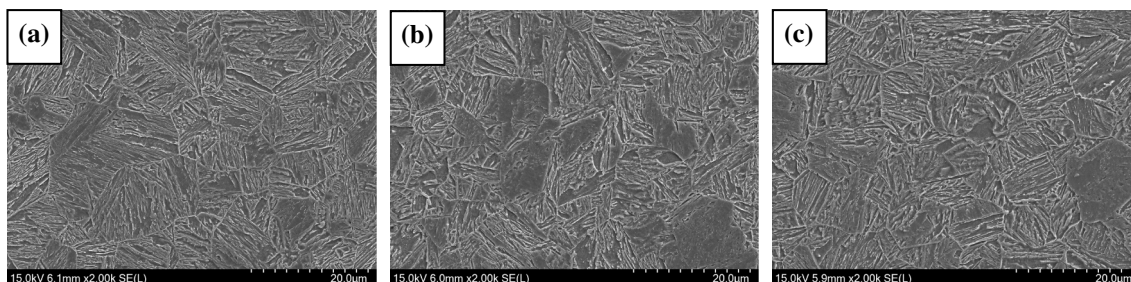


Fig. 6 Microstructure of CGHAZ with different actually welding heat inputs. (a) 1.0 kJ/cm; (b) 1.2 kJ/cm; (c) 1.5 kJ/cm

Similar results were reported in previous relevant studies (Ref 16-18).

The size and fraction of M-A constituent were counted by IPP software with different heat inputs; the results is listed in Table 2. The effect of heat inputs on the size and fraction of M-A constituent is presented in Fig. 8. From Table 2, when the heat input was increased from 8 to 36 kJ/cm, the volume fraction of M-A constituent ( $f_{M-A}$ ) increased from 10.07 to 16.85%, and the length size ( $L$ ) of less than 1  $\mu\text{m}$  in which reduced from 70.79% (8 kJ/cm) to 58.69% (36 kJ/cm). It was indicated that the size of M-A constituent was increased with increasing heat input. Generally, the M-A constituent was considered to be massive shape with a 1-3 value of length ( $L$ )/width ( $W$ ), and it was considered to be strip shape when the ratio was more than 3 (Ref 19). Statistical analysis showed that the shape of M-A constituent had no obvious changes, mostly was massive and the  $f_{M-A}$  was about 75-90%.

During the cooling process in thermal simulation, austenite transformed into lath bainite or bainite ferrite, in which carbon diffused into the austenite without phase transformation at the same time, resulting in an improvement in the austenite stability. When the temperature was less than the initial transformation temperature of martensite, low carbon content transformed into martensite, and carbon-rich austenite was retained at low temperature to form M-A constituent (Ref 18). With the heat input increased, the M-A constituent had three changes such as volume fraction, size and shape. In granular bainite, M-A constituent dispersed in the ferrite matrix. From Fig. 3, the content of granular bainite increased with increasing heat input, such that the volume fraction of M-A constituent increased, which was in accordance with the results of Table 2. Previous studies confirmed that the prior austenite grain size is proportional to the size of M-A constituent (Ref 19, 20). In this study, the heat increased from 8 to 36 kJ/cm, the prior austenite grain size was increased from 17 to 100  $\mu\text{m}$ . Thus, the content of M-A constituent was improved, with a size of more than 1  $\mu\text{m}$ . With the heat input increased, the welding cooling rate was reduced such that phase transformation driving force of austenite reduced. Thus, the carbon was rich in the austenite grain boundaries where the necklace M-A constituent formed as a result when the heat input was more than 15 kJ/cm.

### 3.3 Effect of Heat Input on Hardness and Impact Toughness of CGHAZ

Figure 9 presents the hardness and impact energy of CGHAZ with different heat inputs. With the heat input increased, the hardness and impact energy was reduced, and it was more serious for impact energy (approach to 80%) which was reduced from 233 J of 8 kJ/cm to 2 J of 36 kJ/cm.

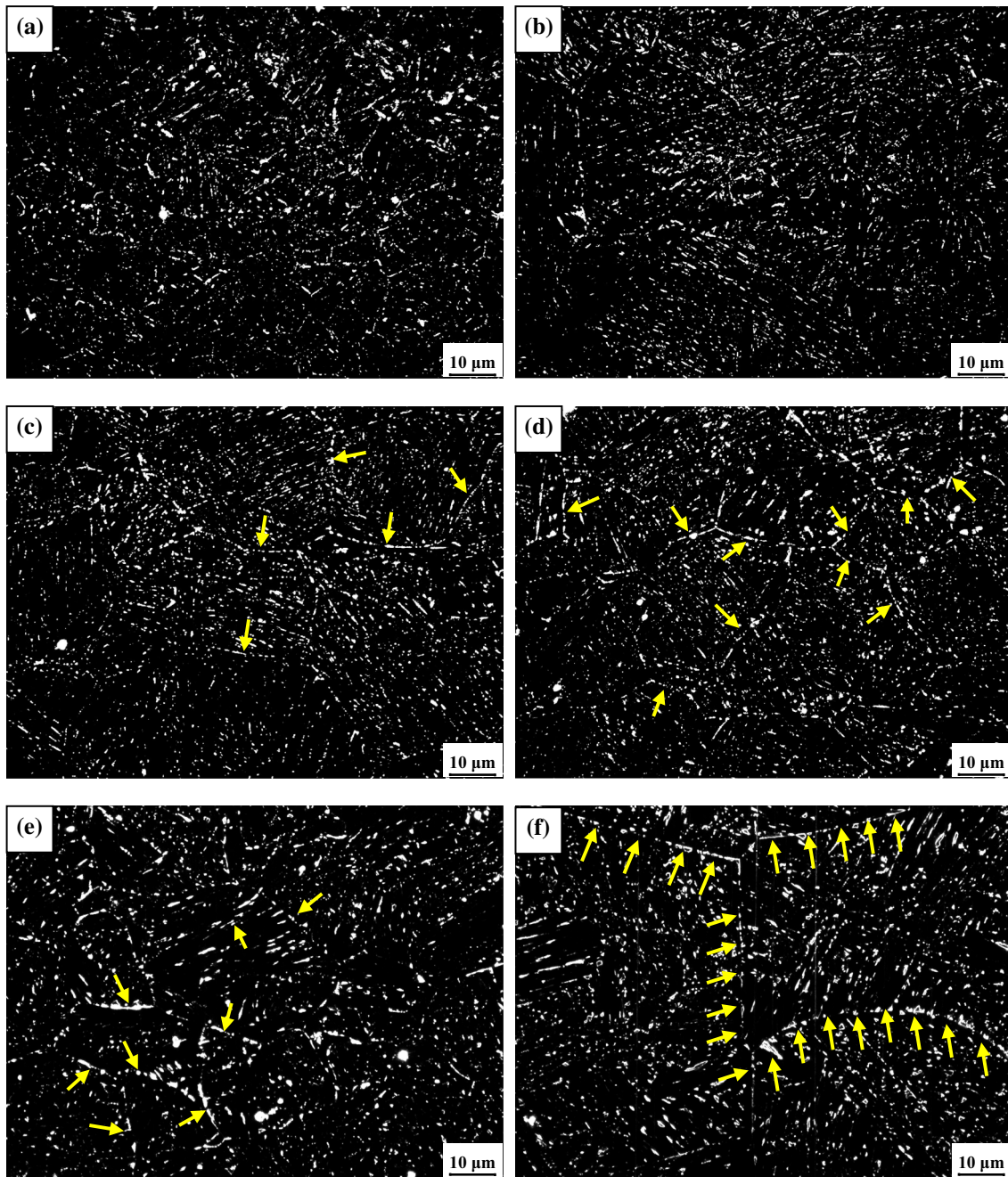


**Fig. 7** Distribution of M-A constituents with different heat inputs. (a) 8 kJ/cm; (b) 10 kJ/cm; (c) 15 kJ/cm; (d) 18 kJ/cm; (e) 26 kJ/cm; (f) 36 kJ/cm

**Table 2** Statistical analysis results of M-A constituent with different heat inputs

<i>E</i> , kJ/cm	8	10	15	18	26	36
$f_{M-A}$ , %	10.07	10.11	10.51	11.62	13.74	16.85
$f_L \geq 1 \mu\text{m}$ , %	29.21	33.39	33.34	28.10	37.15	41.31
$f_L < 1 \mu\text{m}$ , %	70.79	66.61	66.66	71.90	62.85	58.69
$f_{l \leq L/W \leq 3}$ , %	87.25	89.70	89.97	87.92	80.35	74.26
$f_{L/W \geq 3}$ , %	12.75	10.3	10.03	12.08	19.65	25.74

*L*: Size length; *W*: Size width

Compared to the hardness of base metal (BM) (287 HV<sub>0.2</sub>), the highest hardness was 308 HV of 8 kJ/cm and the lowest one was 260 HV of 36 kJ/cm. When the heat input was 15-21 kJ/cm, the hardness was similar to BM. Compared to the impact energy of BM (290 J), it was 233 J with a heat input of 8 kJ/cm that was 80% of BM. With the heat input increased to 36 kJ/cm, the impact energy was only 9% of BM.

Generally, hardness was depended on the microstructure type such as martensite, bainite, ferrite and pearlite (Ref 21). In this study, the M-A constituent and prior austenite grain size changed significantly with the heat input increased, but the

microstructure of CGHAZ was still lath bainite or granular bainite. Thus, the hardness did not fluctuate evidently with heat input increased. However, the reduction in impact energy was very severe due to the M-A constituent and prior austenite grain size, which had been shown in previous studies (Ref 18, 22).

Figure 10 presents the appearance of impact fracture of BM and CGHAZ with different heat inputs. The fracture appearance of BM was uneven with obvious plastic deformation, implying as ductile fracture (Fig. 8a). When the heat input was 26 kJ/cm and 36 kJ/cm, even fracture appearance was observed without deformation, implying as brittle fracture (Fig. 10f and g). For other heat inputs, the fracture mode was between brittle and ductile fracture only with partial plastic deformation.

Figure 11 presents SEM images of impact fracture of BM and CGHAZ with different heat inputs. A large number of dimples were observed in the fracture surface of BM (Fig. 11a).

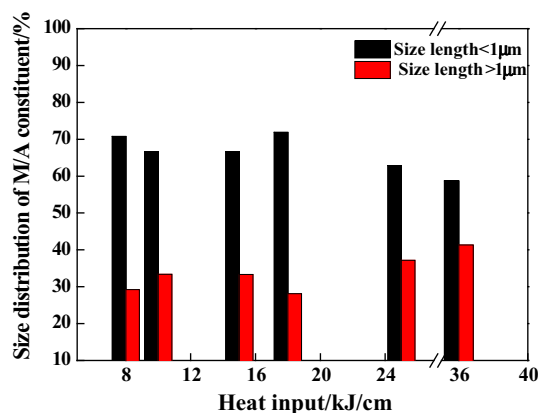


Fig. 8 Effect of heat input on the size of M-A constituents

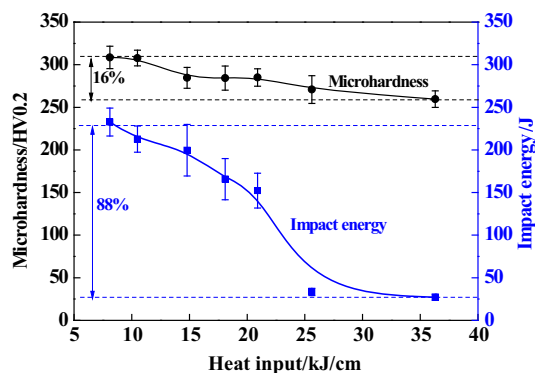


Fig. 9 Hardness and impact energy of CGHAZ with different heat inputs

When the heat input was 8 and 10 kJ/cm, the fracture surface consisted of ductile and brittle fracture zone. One feature of the fracture was the dimples with vary sizes (Fig. 11b and d) in ductile fracture zone, and others was tearing edges and quasi-cleavage facet in brittle fracture zone (Fig. 11c and d). Thus, its fracture mode was ductile and quasi-cleavage fracture. When the heat input was 15 and 18 kJ/cm, the fracture surface consisted of tearing edges and quasi-cleavage facet, which was quasi-cleavage fracture (Fig. 11e and f). When the heat input was 26 and 36 kJ/cm, the fracture with typical fan-shaped river pattern can be observed (as indicated by yellow arrows in Fig. 11g and h), implying as cleavage fracture.

Consequently, the effect of heat input on the impact fracture mode of CGHAZ was: when the heat input was 8 kJ/cm, it was ductile fracture as well as quasi-cleavage fracture; when the heat put was 11-18 kJ/cm, it was quasi-cleavage fracture; when the heat input was 26-36 kJ/cm, it was brittle fracture.

The impact toughness of BM and actual welded joints was test at  $-40^{\circ}\text{C}$  temperature using pendulum impact testing machine (Fig. 12). The laser welding heat input was 1.5 kJ/cm, and the size of impact sample was  $55 \times 10 \times 5$  mm, “V”-notch located in the HAZ near to fusion line (Fig. 12a). The impact fracture surface of this welded joint was showed in Fig. 12(b). Both of the BM and HAZ samples were typical ductile fracture with a great deal of dimples (Fig. 12c and d), but the dimples in HAZ were relatively shallow compared to BM. The impact energy of HAZ was 67 J, 66% of BM (101 J).

For welding thermal simulation, it can be inferred from Fig. 9 that the impact toughness was increased with the reduction in heat input. Thus, the estimated impact toughness of 1.5 kJ/cm was more than 80% (8 kJ/cm) of BM, but it was only 66% in actual welded joints. The reason was that “V”-notch may be between in fusion line and HAZ and the impact toughness of fusion line was the worst region of welded joints, so the impact toughness of HAZ of actual welded joints was lower than the results of welding thermal simulation.

### 3.4 Effect of Heat Input on Secondary Crack of CGHAZ

The crack propagation in impact fracture determined the impact toughness. Primary and secondary crack in impact fracture side surface of BM and CGHAZ with different heat inputs are presented in Fig. 13 (dark region indicated by yellow arrow). For BM, it had good plastic deformation ability due to the bainite microstructure with obvious plastic deformation and the absence of secondary crack (Fig. 13a). When the heat input was 8 and 10 kJ/cm, secondary crack was almost never observed near the primary crack. It showed a relatively good plasticity of its microstructure (Fig. 13b). When the heat input was 26 and 36 kJ/cm, a great deal of secondary crack was observed. The number and width were more than that of other

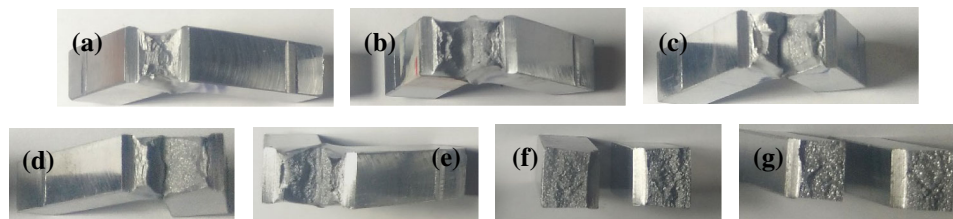
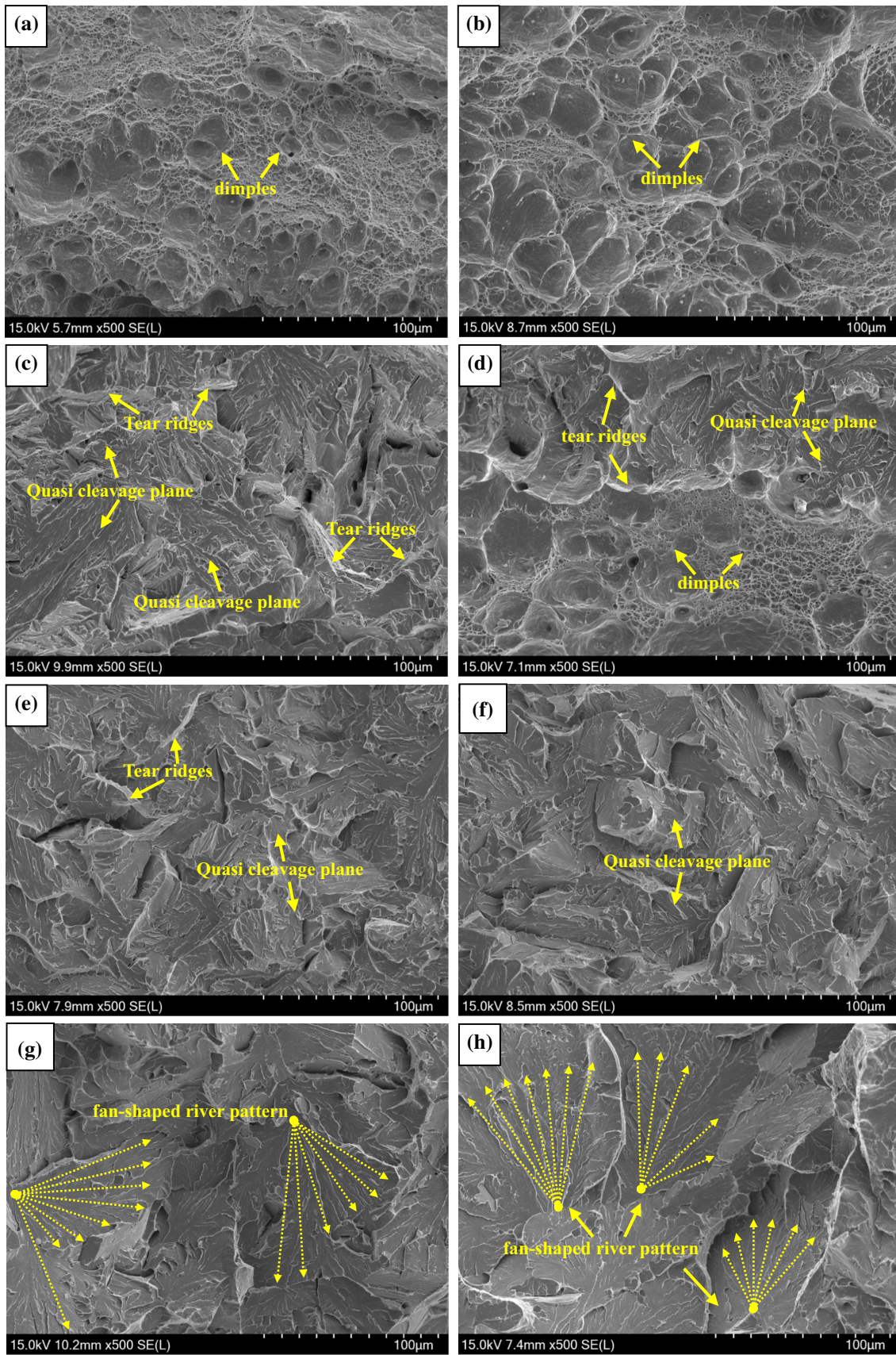
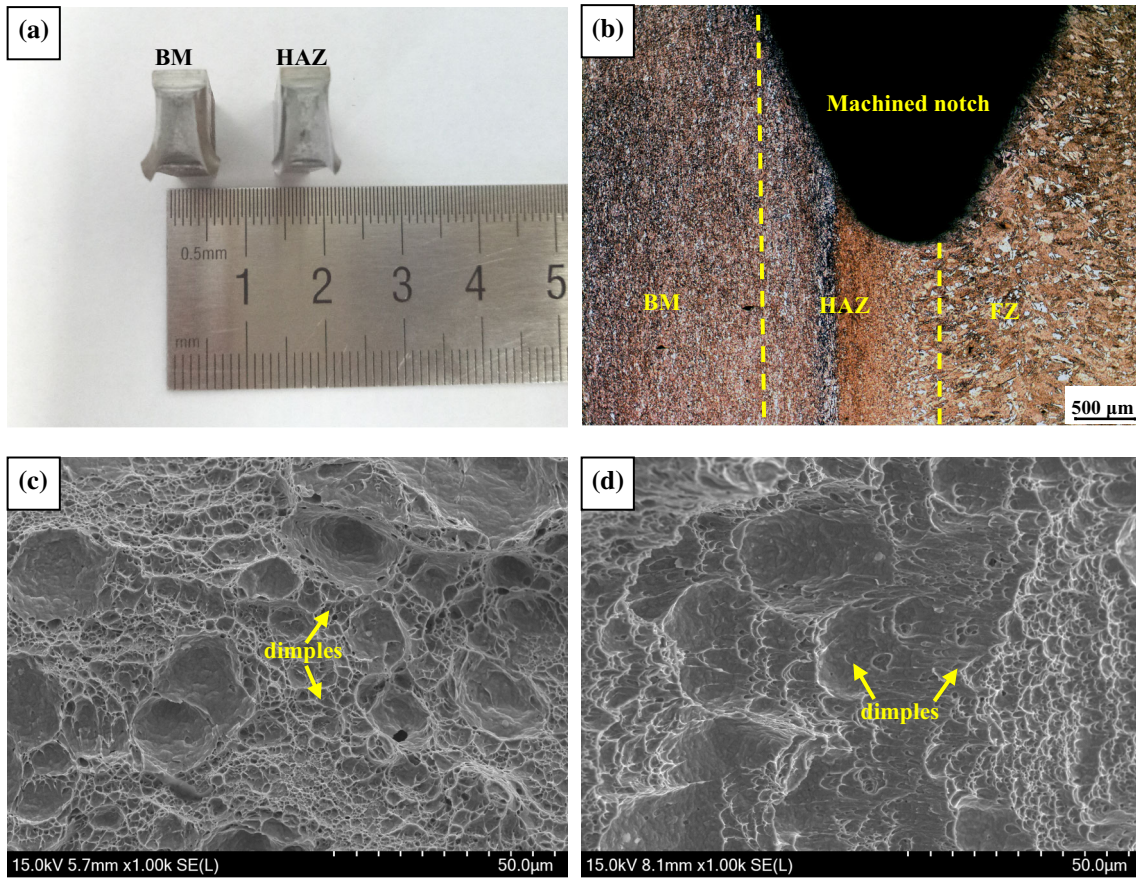


Fig. 10 Appearance of impact fracture of BM and CGHAZ with different heat inputs. (a) BM; (b) 8 kJ/cm; (c) 10 kJ/cm; (d) 15 kJ/cm; (e) 18 kJ/cm; (f) 26 kJ/cm; (g) 36 kJ/cm



**Fig. 11** SEM images of impact fracture of BM and CGHAZ with different heat inputs. (a) BM; (b) (c) 8 kJ/cm; (d) 11 kJ/cm; (e) 15 kJ/cm; (f) 18 kJ/cm; (g) 26 kJ/cm; (h) 36 kJ/cm





**Fig. 12** Impact fracture surface of BM and HAZ of actual welded joints. (a) Micromorphology of BM and HAZ; (b) OM images of HAZ with “V”-notch; (c) Fracture SEM images of BM; (d) Fracture SEM images of HAZ

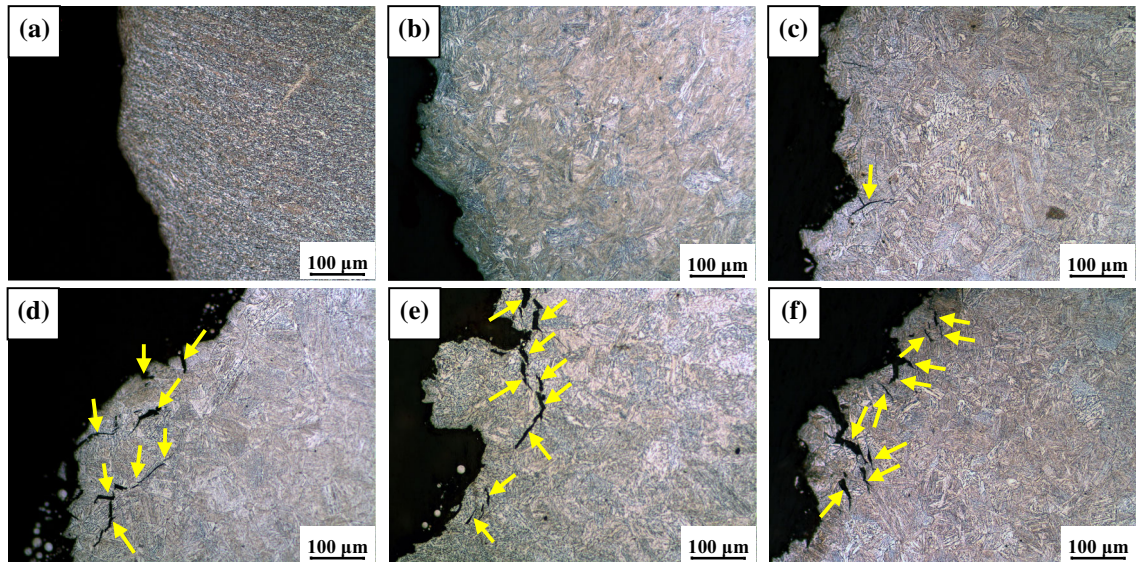


**Fig. 13** Primary and secondary crack in impact fracture side surface of BM and CGHAZ with different heat inputs. (a) BM; (b) 8 kJ/cm; (c) 15 kJ/cm; (d) 18 kJ/cm; (e) 26 kJ/cm; (f) 36 kJ/cm

heat inputs, with the bulk metal falling off (Fig. 13e and f). Thus, the plastic of the microstructure was poor. When the heat input was 15 kJ/cm and 18 kJ/cm, secondary crack was also observed, but its number and size was reduced compared to 26 and 36 kJ/cm (Fig. 13c and d).

Based on the above analysis, with the heat input increased, the number and width of secondary was increased and presented a tendency of the bulk metal falling off, which indicated that the toughness of CGHAZ was getting worse.

Further observation of crack in impact fracture side surface is shown in Fig. 14. When the heat input was 8 kJ/cm, lath bainite with a good plastic presented obvious plastic deformation around the primary crack (Fig. 14a and b). Only a few of secondary cracks with less length can be observed, and the propagation of primary crack was deflected and terminated at the prior austenite grain boundary (PAGB) (Fig. 14b). It was indicated that the crack propagation energy was consumed by PAGB.

When the heat input was more than 15 kJ/cm, the number of secondary crack was increased obviously and size was greater (Fig. 14c, e and g). It was shown that the ability for microstructure to hinder the crack propagation reduced significantly. The crack propagation was also deflected and terminated at PAGB, but the around microstructure had no deformation (Fig. 12d, f and h). Moreover, the interface between M-A constituent and matrix, as well as the PAGB with necklace-like M-A constituent had been the crack initiation and rapid propagation channel (Ref 23).

According to the Griffith formula (Ref 24):

$$\sigma_c = \sqrt{\left(\frac{\pi E \gamma}{(1 - \nu^2) d}\right)} \quad (\text{Eq 3})$$

where  $\sigma_c$  is critical fracture stress,  $E$  is modulus of elasticity,  $\nu$  is Poisson ratio,  $\gamma$  is surface energy of materials,  $d$  is microcrack size, here is maximum length of M-A constituent. In this study, a statistical analysis of  $d$  values was carried out with different heat inputs using IPP software. The results showed that the value of  $d$  was 3.6 and 6.5  $\mu\text{m}$  when the heat input was 8 and 36 kJ/cm, respectively, and the calculated  $\sigma_c$  in the case of 36 kJ/cm was 70% of 8 kJ/cm. It means that the length size of M-A constituent was greater, the critical fracture stress required for microcrack propagation was less, and it was easy to be the crack source during impact process. Previous studies showed that the M-A constituent with the length size of more than 1  $\mu\text{m}$  can become the crack source (Ref 15). From Fig. 8, it can be seen that the number of M-A constituent greater than 1  $\mu\text{m}$  in unit area was increased (29.21%  $\rightarrow$  41.31%) with the heat input increasing (8  $\rightarrow$  36 kJ/cm), leading to the impact toughness reduce.

M-A constituent was also presented in microstructure of BM, but its impact energy was up to 290 J, due to that it dispersed on the ferrite matrix with an average length size of 0.4  $\mu\text{m}$  (maximum was 0.823  $\mu\text{m}$ ). Studies in previous suggested that the M-A constituent with a length size of less than 1  $\mu\text{m}$  and dispersion distribution can not only change the direction of crack propagation but also restrain the crack propagation, such that the toughness was improved (Ref 25, 26).

Moreover, the toughness was also deteriorated by the necklace-like M-A constituents formed in the condition of high heat inputs ( $> 15$  kJ). In Fig. 13, most of secondary crack initiated at the prior austenite grain boundary (PAGB) with necklace-like M-A constituents or propagated along PAGB. The similar results that the toughness of IC-CGHAZ of X100 pipeline steels was less than 50 J due to the presence of necklace-like M-A constituents were found in previous (Ref 27, 28).

Grain boundary was an important factor effected toughness, not only changed the propagation direction of microcracks (Fig. 14d) and even prevented its propagation (Fig. 14b). The relationship between prior austenite grain size and cleavage face was given in Eq 4 (Ref 12):

$$d_c = 2.2 + 0.57d_a \quad (\text{Eq 4})$$

where  $d$  is average size of cleavage face,  $d_a$  is average size of austenite grain. From Eq 4, the size of cleavage face was increased with the austenite grain size increased and toughness was decreased gradually.

Consequently, the reason that the impact toughness of CGHAZ was reduced with heat input increased was concluded as following: first, as the heat input was more than 15 kJ, the necklace-like M-A constituent dispersed on prior austenite grain boundaries was increased gradually where the second crack initiated and grew along it. Second, with the heat input increased (8  $\rightarrow$  36 kJ/cm), the numbers of M-A constituent with a length size of more than 1  $\mu\text{m}$  raised from 29.21 to 41.31%, which resulted in a reduction in impact toughness. Third, with the heat input increased, the prior austenite grain size was improved from 15 to 100  $\mu\text{m}$  such that the impact toughness was deteriorated.

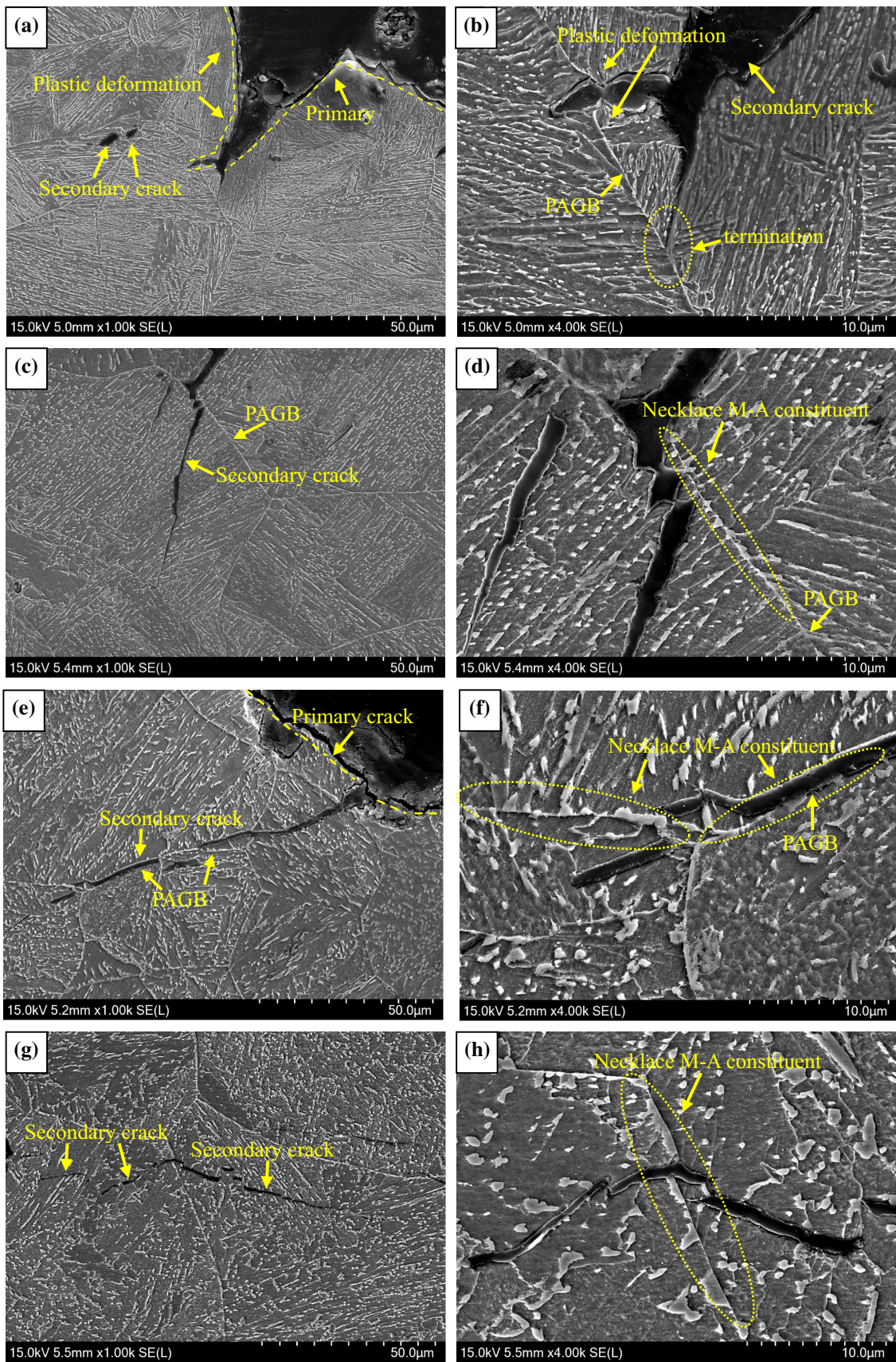
### 3.5 Effect of Heat Input on Corrosion Resistance of CGHAZ

Figure 15 presents the self-etching current density of BM and CGHAZ with different heat inputs. It was showed that with the heat input increased the self-etching current density was increased. That is to say, the corrosion resistance of CGHAZ was reduced with the increasing heat input.

Actually, corrosion is also an electrochemical reaction process. Increasing the microstructure uniformity of steels can reduce the potential difference of anode and cathode, and the corrosion rate is reduced such that local corrosion is slowed down. For the samples of welding thermal simulations, M-A constituents were a carbon-rich phase (carbon content was ten times of matrix) (Ref 13), which was considered as a cathode to establish partial corrosion with readily soluble bainite ferrite (considered as anode). Thus, the corrosion rate was improved. When the heat input was more than 15 kJ/cm, the necklace-like carbon-rich M-A constituent was present at prior austenite grain boundary, which led the increase in grain boundary interfacial energy and further accelerates the corrosion process such that the corrosion resistance gradually decreasing.

## 4. Conclusions

1. When the heat input was 8-18 kJ/cm, the microstructure consisted of lath bainite and granular bainite. With the heat input increased to 26-36 kJ/cm, the microstructure was full granular bainite. The relationship between prior austenite grain size ( $D$ ) and heat input ( $E$ ) was expressed by exponential function,  $D = 0.76 * e^{(E/7.65)} + 15.7$ . This mathematical model can be used to precise predict the grain size at lower heat input conditions such as laser welding.
2. With the heat input increased, three changes were obtained for M-A constituent: First, the volume fraction increased from 10.07% (8 kJ/cm) to 16.85% (36 kJ/cm); second, the numbers of length less than 1  $\mu\text{m}$  were decreased from 70.79% (8 kJ/cm) to 58.69% (36 kJ/cm). Third, when the heat input was more than 15 kJ/cm, the necklace-like M-A constituent formed on prior austenite grain boundaries.
3. The heat input had a little effect on hardness (with a reduction of 16%), but it was obvious on impact toughness (with a reduction of 88%) due to the M-A con-



**Fig. 14** Crack propagation of impact side surface with different heat inputs. (a), (b) 8 kJ/cm (c), (d) 15 kJ/cm; (e), (f) 26 kJ/cm; (g), (h) 36 kJ/cm

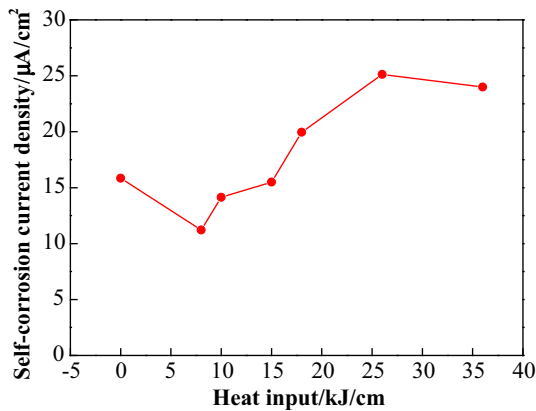


**Fig. 15** Self-etching current density of BM and CGHAZ with different heat inputs

stituent and prior austenite grain size. The corrosion resistance of CGHAZ improved with heat input increased due to electrochemical corrosion of cathode and anode formed by M-A constituent and bainitic ferrite. Thus, the corrosion rate was accelerated with M-A constituent changed.

- The formation of necklace-like M-A constituent at the prior austenite grain boundary can be controlled when the welding heat input was less than 15 kJ/cm, finer M-A constituent dispersing in austenite was obtained. It was advantageous to improve the impact toughness and corrosion resistance of welded joints of X100 pipeline steels.

## Acknowledgments

This work was financially supported by the National Natural Science Foundation of China (No. 51775102), Open Research Fund from the State Key Laboratory of Rolling and Automation, Northeastern University (No. 2016005) and Project Funded by China Postdoctoral Science Foundation (No. 2016M601877).

## Reference

- Z.Y. Lei, Microstructure and Mechanical Properties of Fiber Laser-Metal Active Gas Hybrid Weld of x80 Pipeline Steel, *J. Press Vessel Technol.*, 2013, **135**, p 1–6
- Y. Yang, J.S. Chen, and W.J. Nie, Investigation on the Microstructure and Toughness of Coarse Grained Heat Affected Zone in X-100 Multiphase Pipeline Steel with High Nb Content, *Mater. Sci. Eng. A*, 2012, **558**, p 692–701
- S.K. Sharma and S. Maheshwari, A Review on Welding of High Strength Oil and Gas Pipeline Steels, *J. Natl. Gas Sci. Eng.*, 2017, **38**, p 203–217
- H.B. Cui, G.M. Xie, Z.A. Luo et al., The Microstructural Evolution and Impact Toughness of Nugget Zone in Friction Stir Welded X100 Pipeline Steel, *J. Alloys Compd.*, 2016, **681**, p 426–433
- C.W. Li, Y. Wang, and T. Han, Microstructure and Toughness of Coarse Grain Heat-Affected Zone of Domestic X70 Pipeline Steel During In-Service Welding, *J. Mater. Sci.*, 2011, **46**, p 727–733
- L.G. Lan, C.I. Qiu, D.W. Zhao et al., Microstructural Characteristics and Toughness of the Simulated Coarse Grained Heat Affected Zone of High Strength Low Carbon Bainitic Steel, *Mater. Sci. Eng. A*, 2011, **529**, p 192–200
- A. Lambert-perlade, A.F. Gourgues, J. Besson et al., Mechanisms and Modeling of Cleavage Fracture in Simulated Heat-Affected Zone Microstructures of a High-Strength Low Alloy Steel, *Metall. Mater. Trans.*, 2004, **35A**, p 1039–1053

- P. Mohseni, J.K. Solberg, M. Karlsen et al., Cleavage Fracture Initiation at m-a Constituents in Intercritically Coarse-Grained Heat-Affected Zone of a HSLA Steel, *Metall. Mater. Trans. A*, 2014, **45**, p 384–394
- X. Li, Y. Fan, X. Ma et al., Influence of Martensite-Austenite Constituents Formed at Different Intercritical Temperatures on Toughness, *Mater. Des.*, 2014, **67**, p 457–463
- C.L. Davis and J.E. King, Cleavage Initiation in the Intercritically Reheated Coarse-Grained Heat-Affected Zone: Part I. Fractographic Evidence, *Metall. Mater. Trans. A*, 1994, **25**, p 563–573
- Z. Zhu, J. Han, and H. Li, Influence of Heat Input on Microstructure and Toughness Properties in Simulated CGHAZ of x80 Steel Manufactured Using High-Temperature Processing, *Metall. Mater. Trans. A*, 2015, **46**, p 5467–5475
- B. Guo, L. Fan, Q. Wang et al., The Role of the Bainitic Packet in Control of Impact Toughness in a Simulated CGHAZ of x90 Pipeline Steel, *Metals*, 2016, **6**, p 256–263
- X. Li, C. Shang, X. Ma et al., Elemental Distribution in the Martensite–Austenite Constituent in Intercritically Reheated Coarse-Grained Heat-Affected Zone of a High-Strength Pipeline Steel, *Scr. Mater.*, 2017, **139**, p 67–70
- A. Costa, L. Quintino, D. Yapp et al., Characterization of Fiber Laser Welds in X100 Pipeline Steel, *Mater. Des.*, 2009, **30**, p 2701–2707
- B. Cui, Y. Peng, L. Zhao et al., Effect of Heat Input on Microstructure and Toughness of Coarse Grained Heat Affected Zone of Q890 Steel, *ISIJ Int.*, 2016, **56**, p 132–139
- Y. Gu, P. Tian, X. Wang et al., Non-Isothermal Prior Austenite Grain Growth of a High-Nb X100 Pipeline Steel During a Simulated Welding Heat Cycle Process, *Mater. Des.*, 2016, **89**, p 589–596
- H. Xie, L.-X. Du, J. Hu et al., Effect of Thermo-Mechanical Cycling on the Microstructure and Toughness in the Weld CGHAZ of a Novel High Strength Low Carbon Steel, *Mater. Sci. Eng. A*, 2015, **639**, p 482–488
- L. Lan, C. Qiu, H. Song et al., Correlation of Martensite–Austenite Constituent and Cleavage Crack Initiation in Welding Heat Affected Zone of Low Carbon Bainitic Steel, *Mater. Lett.*, 2014, **125**, p 86–88
- X.D. Li, *Study on the Weldability of the Third Generation Pipeline Steels*, University of Science and Technology Beijing, Beijing, 2015
- E. Bonnevie, G. Ferriere, A. Ikhlefa et al., Morphological Aspects of Martensite–Austenite Constituents in Intercritical and Coarse Grain Heat Affected Zones of Structural Steels, *Mater. Sci. Eng. A*, 2004, **385**, p 352–358
- X.N. Wang, Q. Sun, Z. Zheng et al., Microstructure and Fracture Behavior of Laser Welded Joints of DP Steels with Different Heat Inputs, *Mater. Sci. Eng. A*, 2017, **699**, p 18–25
- S. Kim, D. Kang, T.W. Kim et al., Fatigue Crack Growth Behavior of the Simulated HAZ of 800 MPa Grade High-Performance Steel, *Mater. Sci. Eng. A*, 2011, **528**, p 2331–2338
- X. Li, X. Ma, S.V. Subramanian et al., EBSD Characterization of Secondary Microcracks in the Heat Affected Zone of a X100 Pipeline Steel Weld Joint, *Int. J. Fract.*, 2015, **193**, p 131–139
- D.A. Curry and J.F. Knott, Effects of Microstructure on Cleavage Fracture Stress in Steel, *Metal. Sci.*, 1978, **12**, p 511–514
- Y. Li, D.N. Crowther, M.J.W. Green et al., The Effect of Vanadium and Niobium on the Properties and Microstructure of the Intercritically Reheated Coarse Grained Heat Affected Zone in Low Carbon Microalloyed Steels, *ISIJ Int.*, 2001, **41**, p 46–55
- P. Mohseni, J.K. Solberg, M. Karlsen et al., Investigation of Mechanism of Cleavage Fracture Initiation in Intercritically Coarse Grained Heat Affected Zone of HSLA Steel, *Mater. Sci. Technol.*, 2012, **28**, p 1261–1268
- X.L. Wang, Y.R. Nan, Z.J. Xie et al., Influence of Welding Pass on Microstructure and Toughness in the Reheated Zone of Multi-pass Weld Metal of 550 MPa Offshore Engineering Steel, *Mater. Sci. Eng. A*, 2017, **70(2)**, p 196–205
- X.D. Li, C.J. Shang, C.C. Han et al., Influence of Necklace-Type M-A Constituent on Impact Toughness and Fracture Mechanism in the Heat Affected Zone of X100 Pipeline Steel, *Acta Metall. Sin.*, 2016, **52**, p 1025–1035

**Publisher's Note** Springer Nature remains neutral with regard to jurisdictional claims in published maps and institutional affiliations.